Molecular Plant Pathology WILEY

Protein P5 of pear chlorotic leaf spot-associated virus is a pathogenic factor that suppresses RNA silencing and enhances virus movement

Qiuting Ren[1,2] | Zhe Zhang[2] | Yongle Zhang[2] | Yue Zhang[2] | Yujie Gao[1,2] |
Hongyi Zhang[2] | Xianhong Wang[1,2] | Guoping Wang[1,2] | Ni Hong[1,2] ⬤

[1]Key Laboratory of Plant Pathology of Hubei Province, College of Plant Science and Technology, Huazhong Agricultural University, Wuhan, China

[2]National Key Laboratory for Germplasm Innovation & Utilization of Horticultural Crops, Huazhong Agricultural University, Wuhan, China

Correspondence
Ni Hong, National Key Laboratory for Germplasm Innovation & Utilization of Horticultural Crops, Huazhong Agricultural University, Wuhan 430070, China.
Email: whni@mail.hzau.edu.cn

Abstract

Pear chlorotic leaf spot-associated virus (PCLSaV) is a newly described emaravirus that infects pear trees. The virus genome consists of at least five single-stranded, negative-sense RNAs. The P5 encoded by RNA5 is unique to PCLSaV. In this study, the RNA silencing suppression (RSS) activity of P5 and its subcellular localization were determined in *Nicotiana benthamiana* plants by *Agrobacterium tumefaciens*-mediated expression assays and green fluorescent protein RNA silencing induction. Protein P5 partially suppressed local RNA silencing, strongly suppressed systemic RNA silencing and triggered reactive oxygen species accumulation. The P5 self-interacted and showed subcellular locations in plasmodesmata, endoplasmic reticulum and nucleus. Furthermore, P5 rescued the cell-to-cell movement of a movement defective mutant PVXΔP25 of potato virus X (PVX) and enhanced the pathogenicity of PVX. The N-terminal 1–89 amino acids of the P5 were responsible for the self-interaction ability and RSS activity, for which the signal peptide at positions 1–19 was indispensable. This study demonstrated the function of an emaravirus protein as a pathogenic factor suppressing plant RNA silencing to enhance virus infection and as an enhancer of virus movement.

KEYWORDS
cell-to-cell movement, pear chlorotic leaf spot-associated virus, RNA silencing suppression, signal peptide, subcellular localization, unique protein

1 | INTRODUCTION

The genus *Emaravirus* in the family *Fimoviridae* of the order *Bunyavirales* consists of plant viruses with segmented, single-stranded, negative-sense RNA genomes (Elbeaino et al., 2018; Mielke-Ehret & Mühlbach, 2012). According to the latest ICTV report, there are 29 species and eight tentative species in the genus *Emaravirus* (Digiaro et al., 2024). The infections of most emaraviruses are associated with plant diseases and cause leaf mosaic, chlorotic spots or mottle and fruit malformation (Rehanek et al., 2022). Some emaraviruses are transmitted from plant to plant by eriophyid mites (Acari: Eriophyidae) (Di Bello et al., 2016; Hassan et al., 2017;

Qiuting Ren and Zhe Zhang contributed equally to the study.

McGavin et al., 2012; Mielke-Ehret & Mühlbach, 2012). In infected host plant cells, emaraviruses form double membrane-bounded bodies (DMBs), which are usually associated with host membrane structures (Elbeaino et al., 2018; Guo et al., 2020; Ishikawa et al., 2013; Zheng et al., 2015).

The genomes of emaraviruses consist of 4–10 RNA segments (Elbeaino et al., 2018). Each RNA consists of one open reading frame (ORF) in its complementary RNA strand and two complementary 13-nucleotide (nt) stretches at the 5′ and 3′ termini. RNAs 1–4 encode four core proteins, namely an RNA-dependent RNA polymerase (RdRP), a glycoprotein precursor (GP), a nucleocapsid protein (NC) and a movement protein (MP) (Lu et al., 2015; Mielke-Ehret & Mühlbach, 2012; Mühlbach & Mielke-Ehret, 2012; Tatineni et al., 2014). However, the functions of these proteins are mostly proposed according to their sequence identities with other virus proteins. There are very limited studies on the functions of emaravirus proteins. Initially, protein P4 encoded in the RNA4 strand of raspberry leaf blotch virus (RLBV) was proposed to be an MP based on its plasmodesmatal (PD) location and the secondary structure, which was similar to the 30K superfamily of virus MPs (Yu et al., 2013). The P4 proteins of other emaraviruses are considered to be MPs based on their significant homology with the RLBV P4 protein. Direct experimental evidence is derived from fig mosaic virus (FMV), for which P4 shares the similar subcellular location feature with other viral MPs and has the capacity to complement viral cell-to-cell movement (Ishikawa et al., 2013). Except for the RNA segments encoding the four conserved proteins, the additional RNAs are highly divergent among emaraviruses, suggesting that the proteins encoded in these might have specific functions. However, the functions of these proteins have rarely been studied. The P7 and P8 proteins of High Plains wheat mosaic virus (HPWMoV) independently suppress RNA silencing in *Nicotiana benthamiana*, and the presence of P7 or P8 enhances the pathogenicity of potato virus X (PVX) (Gupta et al., 2018). RNAs 6–8 of RLBV encode three sequence-related proteins, of which P7 and P6 affected the pathogenicity of PVX (Lu et al., 2015).

Pear chlorotic leaf spot-associated virus (PCLSaV) was first discovered in Asian pear (*Pyrus pyrifolia*) trees showing chlorotic leaf spot symptoms in China (Liu et al., 2020). Subsequently, viral infection in *P. pyrifolia* 'Hosui' and *P. communis* 'Le Lectier' was reported in Japan (Kubota et al., 2021). PCLSaV infection causes semitransparent chlorotic spots or chlorotic ringspots on young leaves, accompanied by brown necrosis of the bark of young shoots. These spots become necrotic and severely diseased leaves become distorted. PCLSaV is unevenly distributed in diseased shoots with a high virion accumulation in young leaves (Zhu et al., 2022). The PCLSaV genome consists of five RNA segments, of which RNAs 1–4 encode the core proteins RdRP, GP, NP and MP, respectively. The GP may be converted into two proteins GN and GC according to predicted cleavage sites. Protein P5, encoded by RNA5, is unique to PCLSaV and displays low amino acid (aa) sequence identity (22.9%) with the putative silencing suppressor P7 of HPWMoV, but not with proteins encoded by other emaraviruses and proteins reported in GenBank

(Liu et al., 2020). There is no conserved domain in P5. Therefore, its functions remain to be elucidated.

In this study, we characterized the subcellular localization of PCLSaV P5 and revealed its RNA silencing suppression activity and effects on pathogenicity.

2 | RESULTS

2.1 | PCLSaV P5 is an RNA silencing suppressor

To determine if PCLSaV-encoded proteins can suppress RNA silencing in plant cells, in the initial tests, each of pCNF3 constructs expressing PCLSaV proteins P2 (GP), GN, GC, P3, P4 and P5 along with a 35S:green fluorescent protein (GFP) construct was co-inoculated into young leaves of 4- to 6-week-old plants of *N. benthamiana* line 16c by agroinfiltration (Figure S1a). The P19 construct of tomato bushy stunt virus (TBSV) and the empty pCNF3 vector (EV) were used as positive and negative controls, respectively. At 2 days post-infiltration (dpi), all infiltrated patches of *N. benthamiana* leaves showed bright GFP fluorescence under UV illumination, indicating GFP expression. At 3 dpi, GFP fluorescence was observed in the P5-infiltrated patches, albeit at lower levels compared with P19-infiltrated patches. In contrast, the intensity of green fluorescence was greatly reduced in other infiltrated patches and much weaker GFP fluorescence was observed in the P3-infiltrated patches (Figure S1a,b). Relatively higher GFP levels were detected in P5 and P19 leaf patches by western blot assays (Figure S1b). The P5 and P19 constructs and EV were individually inoculated into the same leaves of *N. benthamiana* 16c plants. Results showed that the green fluorescence signals remained with P5 and P19 leaf patches at 4 dpi but became very weak for P5 patches at 5 dpi (Figure 1a). These data suggested that the PCLSaV P5 might possess local RNA silencing suppression activity. The levels of GFP silencing suppression were assayed by examining the accumulation levels of GFP and mRNA in the infiltrated leaf samples at 3 and 5 dpi by western blot with a GFP-specific antibody and reverse transcription-quantitative PCR (RT-qPCR) assays, respectively (Figure 1b,c). Both GFP and GFP mRNA accumulated at higher levels in leaf patches infiltrated with P5 than that in EV-infiltrated patches, indicating that P5 interfered with GFP-sense transgene-induced silencing. The levels of fluorescence and GFP mRNA accumulation in P5-infiltrated leaf patches were lower compared to P19 infiltration, suggesting that P5 was a relatively weak suppressor of local RNA silencing.

To validate the ability of P5 suppressing systemic silencing, the *N. benthamiana* 16c plants agroinfiltrated with P5 or P19 (a positive control) and 35S:GFP constructs were examined for fluorescent signal in the upper leaves and stems under UV illumination until 35 dpi (Figure 1d). At 17 dpi, infiltration with agrobacteria harbouring P5/35S:GFP and P19/35S:GFP did not result in systemic silencing, but two of 10 EV/35S:GFP-infiltrated plants showed a systemic GFP silencing phenotype with the GFP fluorescence disappearing in leaf veins or becoming weak in systemic leaves. At 27 dpi, infiltration
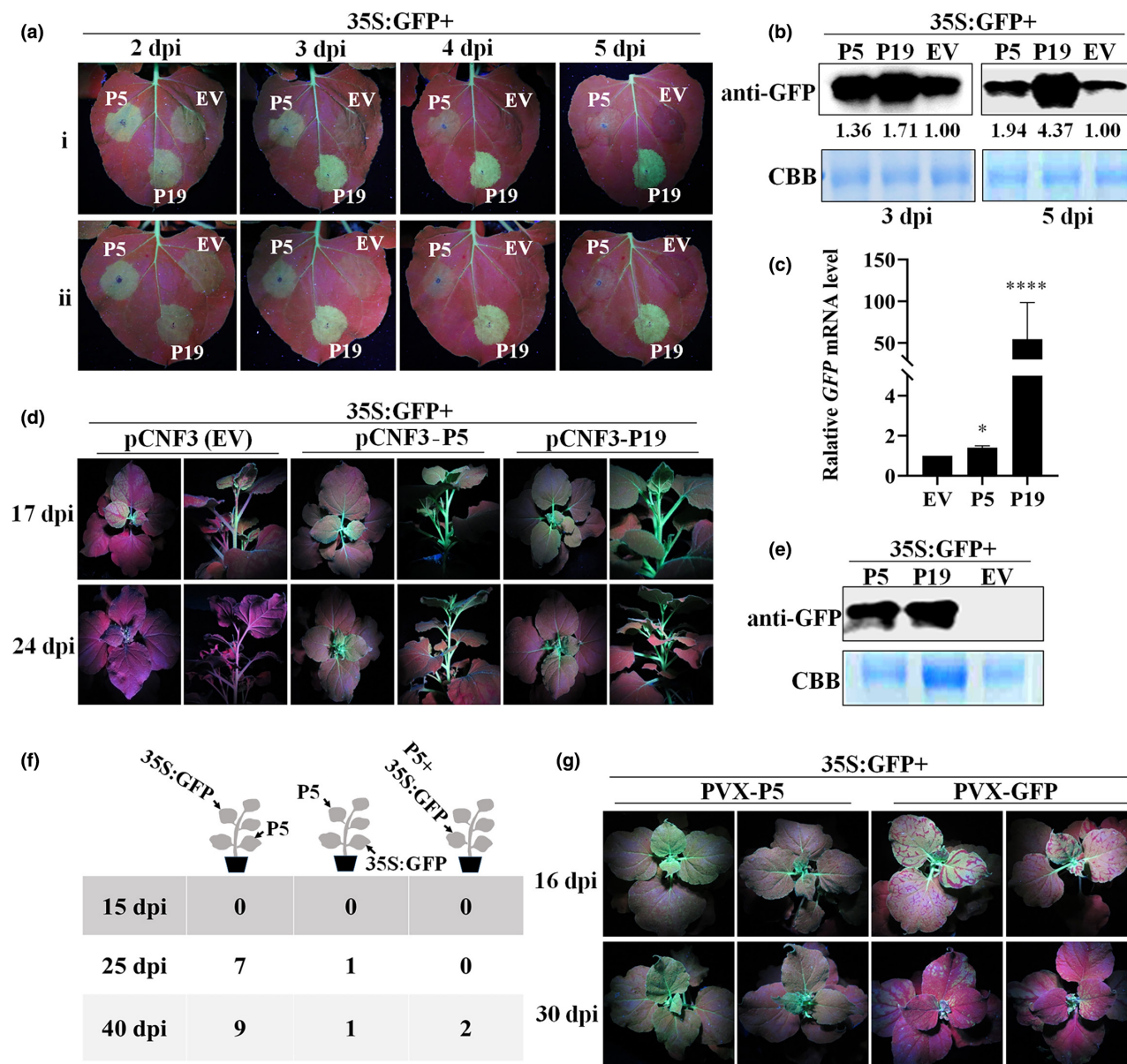
FIGURE 1 Suppression of local and systemic silencing of GFP RNA in *Nicotiana benthamiana* line 16c by PCLSaV P5. (a–c) GFP images and GFP protein and RNA expression levels of infiltrated leaf patches of *N. benthamiana* line 16c. (d, e) GFP images of systemic leaves of *N. benthamiana* line 16c locally expressing P5 and GFP protein expression level in systemic leaves at 30 days post-infiltration (dpi). (f) The GFP-silenced plants out of 10 plants infiltrated with P5 and 35S-GFP inducer at different positions. (g) GFP image of systemic leaves of *N. benthamiana* line 16c systemically expressing P5. In (a–e), TBSV P19 was used as a positive control and the empty vector (EV) was used as a negative control. In (g), PVX-GFP was used as a negative control. The large subunit of RuBisCO stained with Coomassie brilliant blue (CBB) is used as protein loading controls in western blot assays.

with EV/35S:GFP resulted in a systemic silencing phenotype of all plants with GFP fluorescence disappearing in whole plants, but 83.3% (25/30) and 58.3% (7/12) plants infiltrated with P5/35S:GFP and P19/35S:GFP, respectively, did not exhibit systemic silencing. At 35 dpi, 60% P5/35S:GFP and 50% P19/35S:GFP-infiltrated plants had no systemic silencing (Table S1). Nevertheless, western blot assays showed that P5/35S:GFP and P19/35S:GFP infiltrations greatly increased the GFP amount in apical leaves, but GFP was almost completely silenced in the apical leaves of plants infiltrated with EV/35S:GFP (Figure 1e). In addition, P5/35S:GFP-infiltrated plants

had relatively weaker systemic silencing and higher GFP accumulation compared with P19/35:GFP plants, suggesting that P5 had a strong ability for suppressing systemic RNA silencing.

To determine whether P5 could suppress systemic silencing by blocking the mobile inducers of RNA silencing, agrobacteria harbouring P5 and 35S:GFP were infiltrated into *N. benthamiana* leaves at different positions as depicted in Figure 1f. The GFP fluorescence signal in the upper non-infiltrated leaves of *N. benthamiana* plants was examined under UV illumination. At 15 dpi, no systemic silencing was observed in any of the infiltrated plants. At 25 and 40 dpi,

seven and nine plants infiltrated with 35S:GFP in an upper leaf and the P5 construct in a lower leaf showed systemic silencing. In contrast, only one plant infiltrated with 35S:GFP in a lower leaf and the P5 construct in an upper leaf showed systemic silencing signal, and two plants co-infiltrated with P5 and 35S:GFP showed systemic silencing until 40 dpi (Figure 1f). These results indicated that P5 efficiently suppressed systemic silencing by blocking the spread of silencing inducing signals towards apical leaves.

The P5 and GFP were individually cloned into a PVX expression vector. The constructs were individually co-infiltrated with 35S:GFP into leaves of *N. benthamiana* 16c plants. At 16 dpi, PVX-GFP/35S:GFP-infiltrated plants became systemically silenced by showing leaf vein reddening and fully systemically silenced with whole leaves becoming red at 30 dpi. In contract, strong fluorescence persisted in leaves of PVX-P5/35S:GFP-infiltrated plants until 30 dpi (Figure 1g). The results indicated that the systemically expressed P5 efficiently suppressed systemic silencing in *N. benthamiana* 16c plants.

2.2 | PCLSaV P5 suppresses dsRNA-mediated RNA silencing

To examine the efficiency of P5 in suppressing double-stranded (ds) and single-stranded (ss) RNA-induced RNA silencing, agrobacteria with 35S:dsGFP and 35S:ssGFP were separately co-infiltrated with 35S:GFP (reporter gene) and pCNF3-P5 or pCNF3-P19 (a positive control) or EV (a negative control) into *N. benthamiana* 16c leaves (Figure 2a,b). At 2 dpi, GFP fluorescence was observed in all infiltrated leaf patches. At 3–4 dpi, the GFP fluorescence in EV-infiltrated patches became weaker than that in P5- or P19-infiltrated patches. After 5 dpi, the GFP fluorescence was almost completely silenced in P5- or EV-infiltrated leaf patches, but was still observed in P19-infiltrated leaf patches (Figure 2a). In leaf patches co-infiltrated with P5/35S:dsGFP, the accumulation levels of GFP and its mRNA were higher than that in EV-infiltrated leaf patches, but lower than that in P19-infiltrated leaf patches at 3 dpi, and significantly reduced at 6 dpi (Figure 2a). When these constructs were co-infiltrated
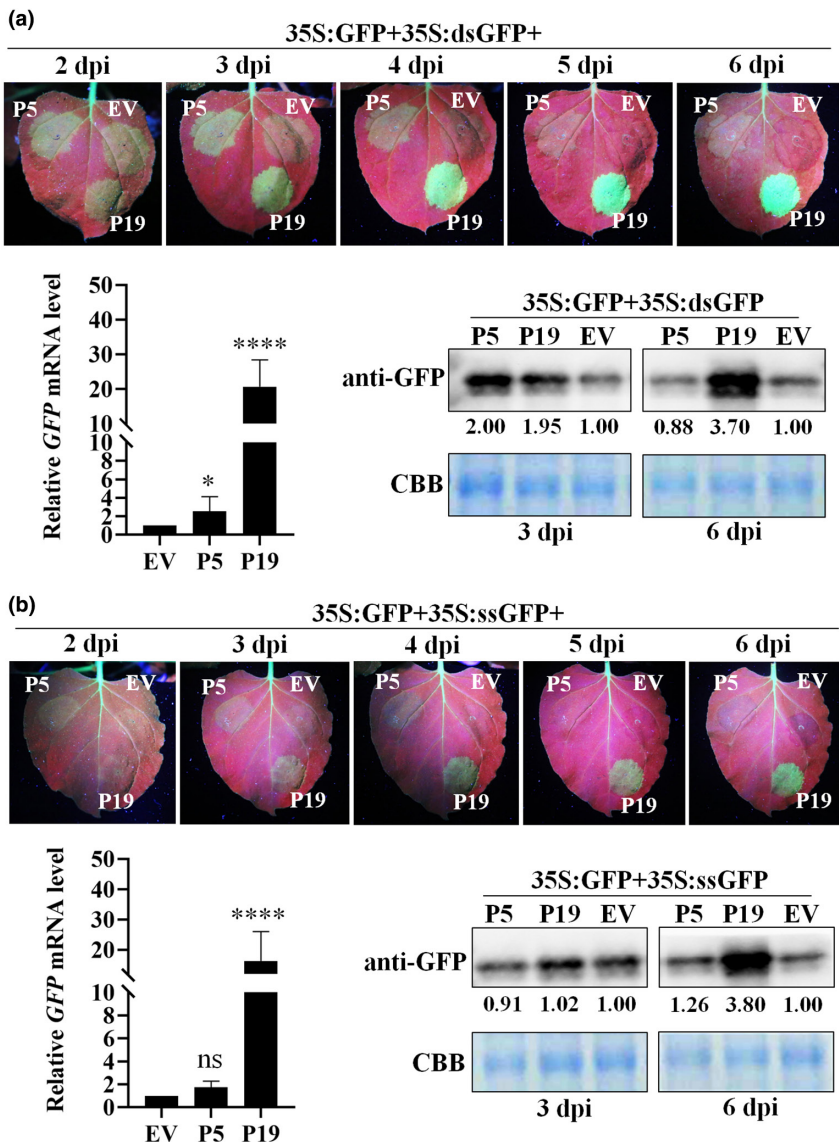

FIGURE 2 P5 suppresses local silencing induced by GFP double-stranded (ds) and single-stranded (ss) RNAs in *Nicotiana benthamiana* line 16c. (a) GFP images, GFP protein and RNA expression levels of leaf patches of *N. benthamiana* line 16c agroinfiltrated with 35S-GFP and 35S-dsGFP combined with each of P5, P19 (a positive control), and an empty vector (EV, a negative control) at 2–6 days post-infiltration (dpi). (b) GFP images, GFP protein and RNA expression levels of leaf patches of *N. benthamiana* line 16c agroinfiltrated with 35S-GFP and 35S-ssGFP combined with each of P5, P19 and EV, a negative control at 2–6 dpi. GFP protein expression levels were detected by western blot at 3 and 6 dpi and quantified by using ImageJ. The large subunit of RuBisCO stained with Coomassie brilliant blue (CBB) is used as a protein loading control. The relative accumulation levels of GFP mRNA in agroinfiltrated leaf patches were analysed by reverse transcription-quantitative PCR at 3 dpi. The expression levels of GFP mRNA were normalized to *NbGAPDH* mRNA levels. Values were means $\pm$ *SD* from three independent experiments. ns, no significance. *$p < 0.05$, ****$p < 0.0001$.

with 35S::ssGFP, the GFP fluorescence disappeared in patches co-infiltrated with P5 or EV at 3–6 dpi, and the accumulation levels of GFP and its mRNA in P5-infiltrated leaf patches were not significantly different than those in EV-infiltrated leaf patches (Figure 2b). These results indicated that P5 suppresses dsRNA-mediated but not ssRNA-mediated RNA silencing and has a mild silencing suppression activity at the local level as compared with P19.

2.3 | PCLSaV P5 triggers accumulation of reactive oxygen species in *N. benthamiana* leaves

Intriguingly, during the above tests, chlorotic necrosis was observed in the leaf patches infiltrated with P5/35S:GFP of *N. benthamiana* 16c at 3 dpi. The chlorosis became more clear at 5 dpi, and the opposite underside faces of the infiltrated patches had epidemical

films separated from leaf tissues, which was never observed in EV/35S:GFP-infiltrated patches (Figure S2). Furthermore, when the P5 was expressed in wild-type *N. benthamiana* leaves, the same chlorotic necrosis and epidemical films were induced (Figure 3a,b).

To assess whether the necrosis induction was correlated with reactive oxygen species (ROS) accumulation triggered by PCLSaV P5 in plants, we used 3,3′-diaminobenzidine tetrahydrochloride (DAB) and nitroblue tetrazolium (NBT) staining to detect the levels of hydrogen peroxide (H_2O_2) and superoxide anion (O^-_2) in *N. benthamiana* leaves. A dark brown colour developed in the DAB-stained P5-infiltrated samples compared to the light-yellow colour in the EV-inoculated samples (Figure 3c). Similarly, application of NBT showed the development of a blue staining in P5-infiltrated samples, but no or very weak blue staining in the EV control samples (Figure 3d). Accordingly, the H_2O_2 content significantly increased in the P5-inoculated leaves as compared with that in EV-inoculated
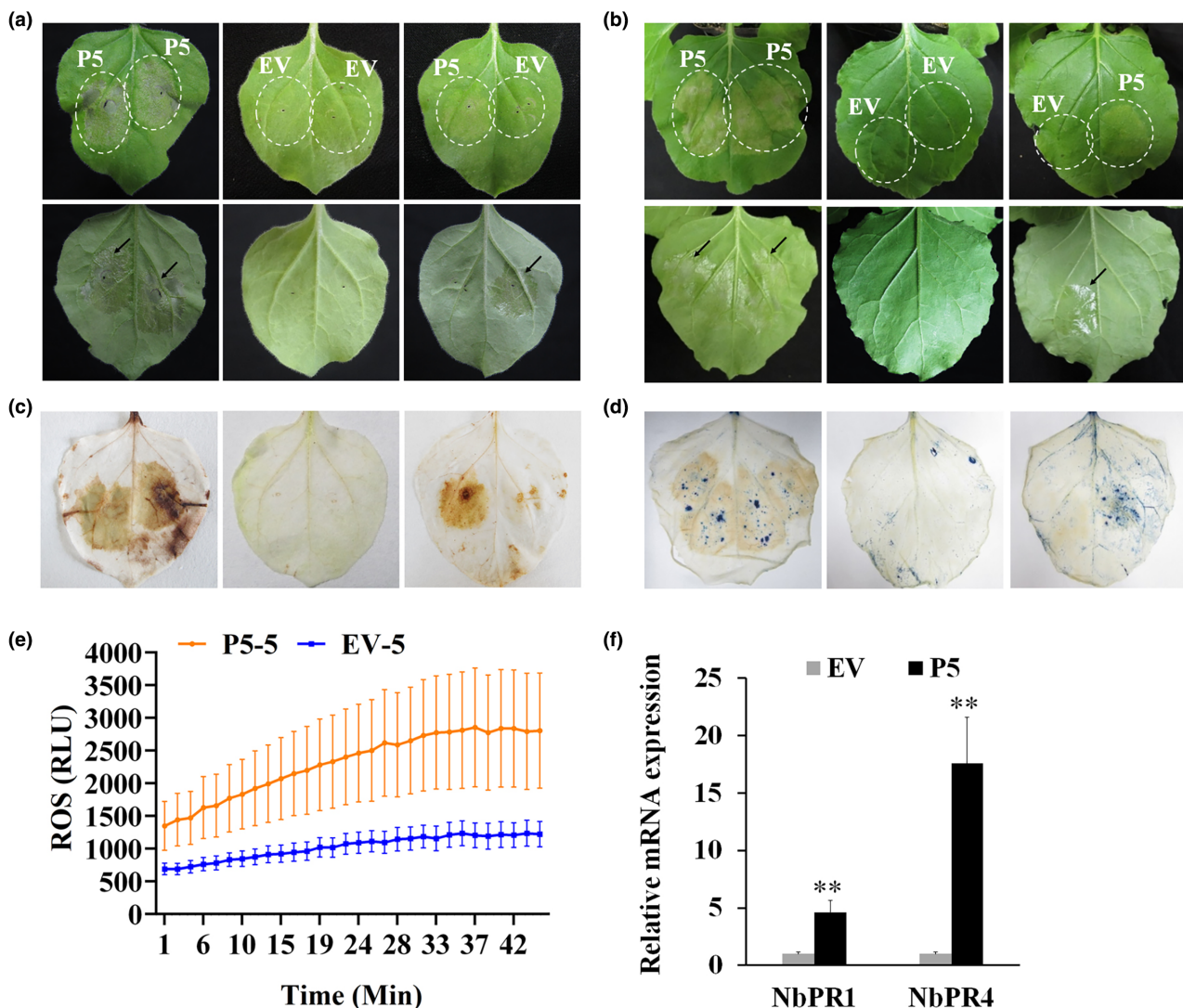

FIGURE 3 P5 induces leaf necrosis, reactive oxygen species accumulation and PR gene expression in *Nicotiana benthamiana* leaves. (a, b) The phenotype of *N. benthamiana* leaves (upper panel, front; lower panel, back). (c, d) The 3,3′-diaminobenzidine (DAB) (left) and trypan blue (right) staining of leaves in (a, b). (e, f) The reactive oxygen species accumulation and the transcript levels of NbPR1 and NbPR4 induced by P5 in *N. benthamiana* leaf patches. Significant difference, **$p < 0.01$.

leaves (Figure 3e). These results indicated that the P5 possesses the ability to induce peroxisomal ROS accumulation in the infiltrated *N. benthamiana* leaves. RT-qPCR analysis demonstrated that the *N. benthamiana* NbPR1 and NbPR4 genes involved in the salicylic acid (SA) signalling pathway were significantly upregulated 4.6 and 17.6 times in P5-infiltrated leaf patches, respectively. At the same time, the two genes showed almost no response to EV infiltration (Figure 3f). These results suggested that the P5 could be one of the viral factors that triggers the host immune response.

2.4 | PCLSaV P5 is self-interacting and accumulates in the nucleus, plasmodesmata and endoplasmic reticulum

The presence of P5 in PCLSaV with no homologue in other viruses makes it particularly interesting to determine its major subcellular accumulation sites. For this purpose, the PCLSaV ORF5 was cloned into the vector pEarlyGate101-eYFP and agroinfiltrated into *N. benthamiana* leaves. The infiltrated leaf patches were exanimated by confocal laser scanning microscopy at 2 dpi. The P5-YFP fusion protein, regardless of whether P5 was fused to the N or C terminus of YFP, preferentially accumulated in the nucleus as numerous peripheral nuclear aggregates (nuclear bodies, NB), in plasmodesmata (PD) as discontinuous parallel dots and along endoplasmic reticulum (ER) networks (Figure 4a). The subcellular location features were confirmed by the co-expression of the P5-YFP with nucleus, PD and ER marker proteins H2B-mCherry, CMV 3a-mCherry and mCherry-HDEL, respectively (Figure 4b). When fluorescence signals were captured at different leaf cell layers, the P5-YFP fluorescence signal was also observed to accumulate in ER in the cytoplasm and notably overlapped with the red fluorescence of the ER marker protein mCherry-HDEL (Figure 4b). Moreover, many vesicle-like structures located within the ER membrane. These location features were different from the nucleus and cytoplasm locations of free YFP and the even distribution along ER networks of the ER marker protein mCherry-HDEL (Figure S3). The results indicated that P5 is a protein with multiple locations, which might be associated with specific functions.

Primarily, the self-interaction of the P5 was tested by using the Matchmaker gold yeast two-hybrid (GYTH) system (Clontech) and the split-ubiquitin-based membrane yeast two-hybrid (MYTH) system (Thaminy et al., 2003). Results showed that the P5-BD in GYTH system and MYTH system had transcriptional activation activity in the absence of an interacting partner (Figure S4a,b). The homologous interaction of P5 was tested by bimolecular fluorescence complementation (BiFC) assays and luciferase complementation imaging (LCI) in the epidermal cells of *N. benthamiana* leaves. In the tests, the P5 constructs paired with the corresponding empty vector did not produce a fluorescent signal (Figure S4c,d). At 48 h post-infiltration (hpi), a homologous interaction signal of P5 in the BiFC assay was observed in the infiltrated cells in nuclei, as paired discontinuous spots along cell membranes and along ER networks (Figure 4c), which

matched the signals of nucleus, PD and ER marker proteins H2B-mCherry, CMV 3a-mCherry and mCherry-HDEL well (Figure 4d), and were in accordance with the P5 subcellular locations. LCI assays showed that a luminescent signal produced in the *N. benthamiana* leaf patches co-expressing P5-nLUC and cLUC-P5 (Figure S4d), confirming the self-interaction of P5.

2.5 | PCLSaV P5 rescues the cell-to-cell movement of PVXΔP25-GFP and enhances the pathogenicity of PVX

The PD location of P5 suggested that the protein might function in viral movement. The viral P4 was assumed to be the movement protein according to its sequence similarity with other emaravirus MPs (Liu et al., 2020). Here, we performed BiFC assays to investigate whether P5 could interact and co-localize with P4. Results showed that two proteins interacted with each other with fluorescent signal at PD, but not at ER and nucleus, which was in consistent with the P4 location (Figure 5a). The result indicated that the viral P4 partially changed the subcellular distribution of P5 from ER and nucleus to PD. Furthermore, we investigated the effects of P5 on the cell-to-cell trafficking ability of a movement defective mutant PVXΔP25-GFP. The P4 was also included in the test. A plasmid expressing the heterologous silencing suppressor P19 was co-delivered with PVXΔP25-GFP to enhance the PVXΔP25-GFP expression, as previously reported (Feng et al., 2019; Ganesan et al., 2013; Qian et al., 2017). In the pretests, an *Agrobacterium tumefaciens* culture containing the construct P19 with an OD_{600nm} of 0.5 was co-infiltrated with a serially diluted *Agrobacterium* culture containing PVXΔP25-GFP into *N. benthamiana* leaves. At 3 dpi, the PVXΔP25-GFP cultures with OD_{600nm} of 0.0005, 0.00025 and 0.00001 consistently produced a GFP signal in single cells, as viewed under a scanning confocal microscope. At 5 dpi, the signal distribution did not change but the signal density increased (Figure S5). Then, the PVXΔP25-GFP culture with an OD_{600nm} of 0.00025 was used in the following tests. *Agrobacterium* cultures containing constructs expressing unlabelled P5 and P4 were individually co-infiltrated with cultures containing PVXΔP25-GFP and P19 into *N. benthamiana* leaves. The co-infiltration with a culture containing an empty vector and the cultures containing PVXΔP25-GFP/P19 were used as a control. Scanning confocal microscope observation showed that the fluorescence signal of PVXΔP25-GFP/P19/EV was visible in single cells at 3 dpi and became extensive, but still restricted in single cells, at 5 and 6 dpi (Figure 5b). In contrast, when P4 and P5 were individually co-expressed with PVX-ΔP25-GFP/P19, weak signals spread from the initial infiltrated cells to the adjacent cells at 3 dpi and spread to more connected cells and formed fluorescence-labelled cell clusters with ratios of 79% (19/24) and 95% (21/22), respectively (Figure 5b), indicating that the P5 and P4 of PCLSaV helped the PVXΔP25-GFP cell-to-cell movement.

To investigate whether P5 could enhance viral accumulation, *Agrobacterium* cultures containing the constructs PVX-P5 and
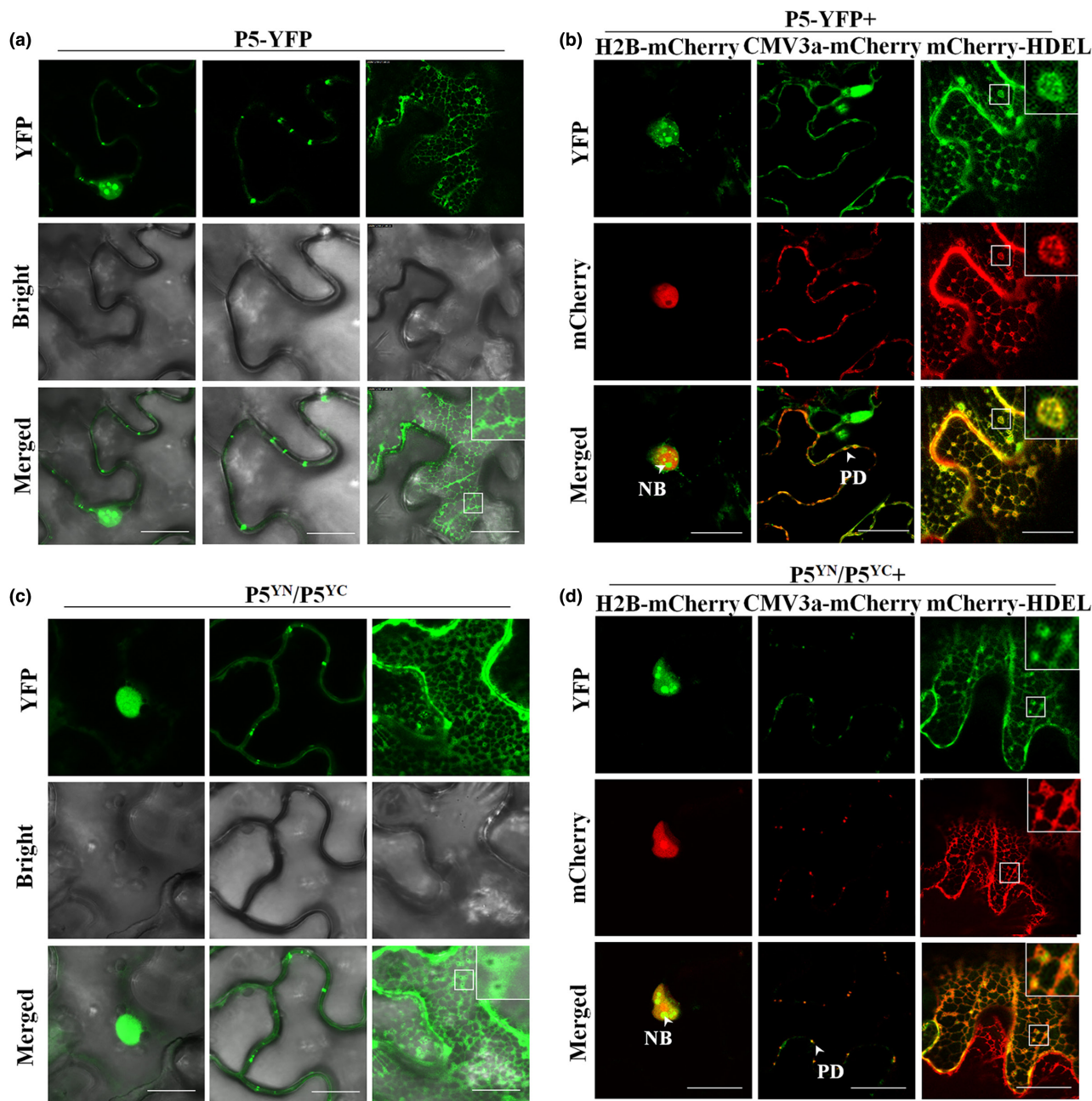
FIGURE 4 Subcellular distribution and its self-interaction of PCLSaV P5 detected by bimolecular fluorescence complementation analysis. (a, b) The subcellular localizations of P5 without and with plasmodesmata, nuclear and endoplasmic reticulum markers CMV3a-mCherry, H2B-mCherry and mCherry-HDEL. (c, d) Bimolecular fluorescence complementation analysis for P5 self-interaction and the colocalization of the interaction signals with CMV3a-mCherry, H2B-mCherry and mCherry-HDEL. The vesicle structures developed from the endoplasmic reticulum (ER) are highlighted in the boxes. NB, nucleus body; PD, plasmodesmata. Images were acquired at 48h after agroinfiltration under a confocal microscope using a 63×/1.20 water objective. Scale bars=20μm.

PVX-GFP were individually infiltrated into *N. benthamiana* leaves. At 7 dpi, the infiltrated plants showed mild leaf mosaic symptoms on the upper non-inoculated leaves. At 14–21 dpi, as compared with PVX-GFP-infected plants, PVX-P5-infected plants showed more severe leaf vein clearing and mottling or mosaic symptoms (Figure 5c). Accordingly, more extensive DAB staining dark-brown colour was observed, and increased PVX CP levels were detected in the PVX-P5-infected plants as compared with those in the PVX- GFP-infected control plants (Figure 5c,d). The results suggested that the

expression of P5 caused necrosis by generating H_2O_2 in *N. benthamiana* leaves, which might improve PVX accumulation.

2.6 | Dissection of the nuclear localization signal and signal peptide of PCLSaV P5

The P5 from PCLSaV isolate CG1 consists of 282 amino acids (aa). Sequence analyses revealed one nuclear localization signal (NLS)
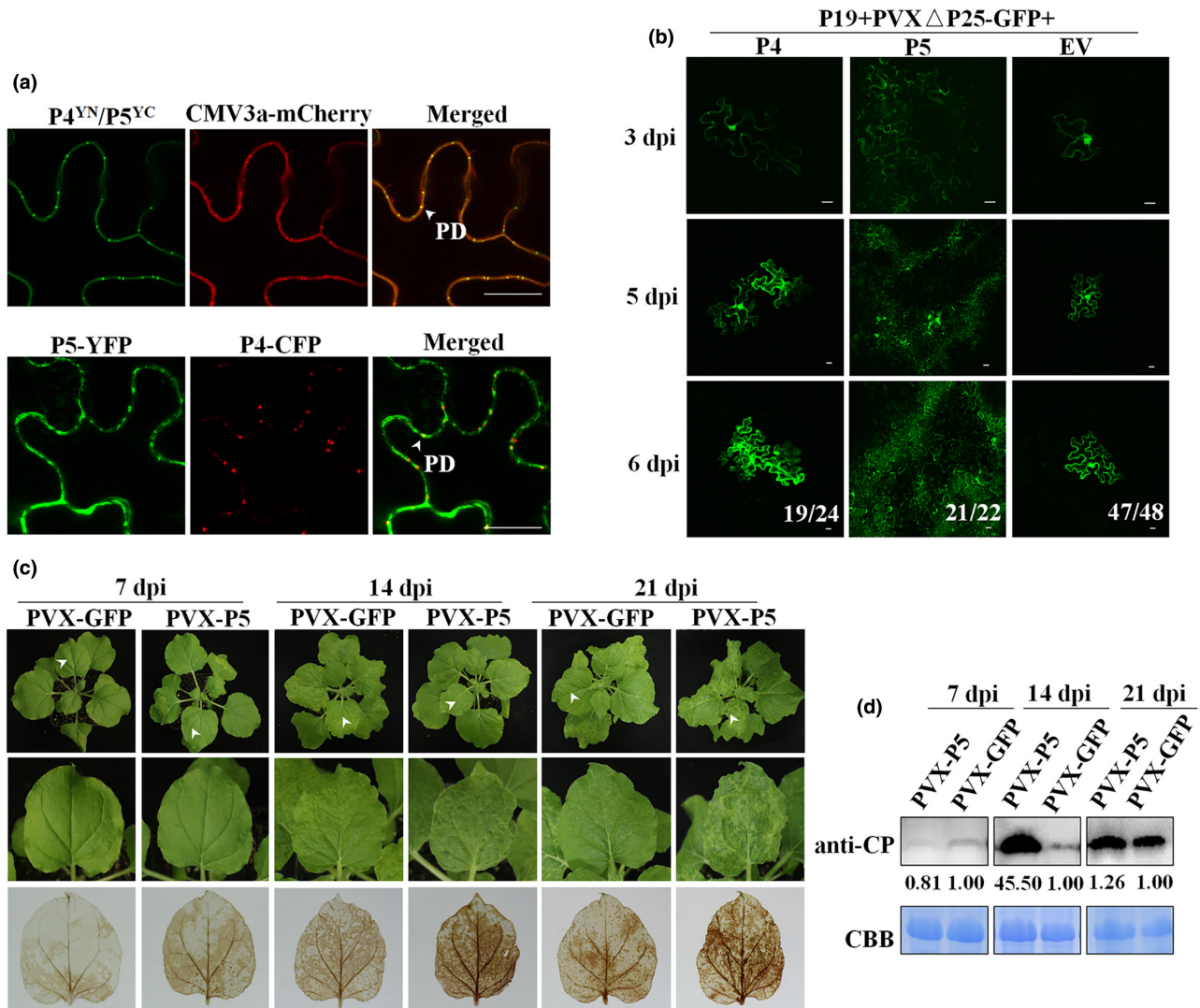
FIGURE 5 PCLSaV P5 interacts and colocalizes with the viral P4 and enhances PVX infection and cell-to-cell diffusion of PVXΔP25-GFP in *Nicotiana benthamiana*. (a) The interaction and colocalization signals of PCLSaV P5 with the viral P4. CMV3a-mCherry was used as a plasmodesmata (PD) marker. (b) The signals of PVXΔP25-GFP in epidermal cells of *N. benthamiana*, in which P5, P4 and an empty vector (EV) were, respectively, co-expressed with PVXΔP25-GFP and P19. Data are presented as views with GFP signal diffused in adjacent cells/total views (P4 and P5) or views with GFP signal in single cell/total views (EV). Scale bars = 10 μm. (c) The symptoms of *N. benthamiana* plants agro-inoculated with PVX-P5 and PVX-GFP at 7–21 days post-infiltration (dpi) and the 3,3′-diaminobenzidine (DAB) staining dark-brown colour. Arrow heads indicated the enlarged leaves. (d) PVX CP expression levels in the young leaves of plants in (c) were detected by western blot. The large subunit of RuBisCO stained with Coomassie brilliant blue (CBB) is used as protein loading controls.

located at positions 203–222 aa or 203–233 aa of P5 as predicated by using NLS tradamus (http://www.moseslab.csb.utoronto.ca/NLStradamus/) or cNLS Mapper (http://nls-mapper.iab.keio.ac.jp/cgi-bin/NLS_Mapper_form.cgi). One potential signal peptide (SP) at positions 1–19 aa with 98.6% possibility was predicted using online software at https://www.novopro.cn/tools/signalp (Figure S6a).

To confirm the presence of an SP in P5, the predicted SP-encoding sequence (1–19 aa), full-length P5-encoding sequence and P5-encoding sequence with a deletion of 1–19 aa (P5$_{\Delta 1-19}$) were constructed into the vector pSUC2 and transformed into the yeast YTK12 (Figure 6a). The transformants with pSUC2-P5$_{1-19}$, pSUC2-P5 and the positive control pSUC2-Avr1bSP had secreted invertase activity and were able to grow well on the YPRAA

medium. However, the transformant with pSUC2-P5$_{\Delta 1-19}$ did not have secreted invertase activity and was unable to grow well on the YPRAA medium, similar to the negative control YTK12 and pSUC2. The results indicated that the SP of P5 has a secretion function.

The preferential accumulation of P5 in the nucleus suggested that the protein might be transported to the nucleus via an importin pathway (Goldfarb et al., 2004; Lange et al., 2007). Then, BiFC assays were performed to test interactions between P5 and each of the two importing proteins NbImpα1 and NbImpα2. The experiments showed that cells co-expressing P5 with Impα1 or Impα2, regardless of their fusion at the N or C terminus of YFP, produced fluorescence signals in the nucleus with numerous

FIGURE 6 Secretion activity and nucleus importin analysis of PCLSaV P5. (a) Secretion activity analysis in TTC medium and yeast growth on CMD−W or YPRAA plates. The yeast mutant YTK12 and its transformant with empty vector pSUC2 were used as negative controls. The yeast transformant with pSUC2-Avr1 was used as a positive control. (b) Interaction signals of P5 and nuclear localization signal (NLS) deletion mutant P5Δ203−222 with NbImpα1 or NbImpα2. (c) Interaction signals of P5 with nucleolus fibrillarin protein Fib2. N, nucleus; NB, nucleus body; NO, nucleolus. Scale bars = 20 μm.
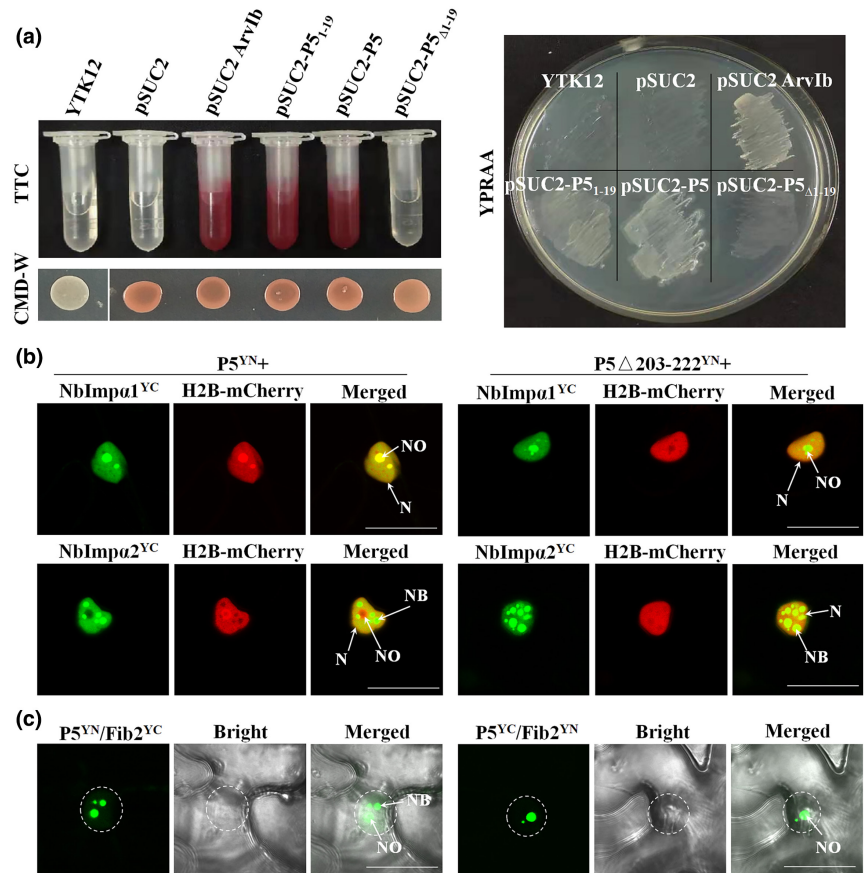
NBs (Figure 6b), suggesting that P5 nuclear transport might rely on the importin α pathway. It was noticed that the fluorescence signal of P5/Impα1 accumulated preferentially in the nucleoplasm and nucleolus, and the fluorescence signal of P5/Impα2 accumulated preferentially in the nucleoplasm as NBs with different sizes, but not in the nucleolus, which was similar to the distribution of P5 in the nucleus. However, the deletion of the potential NLS at 203−222 aa (P5Δ203−222) did not change the nuclear location of the interaction signals between P5 with Impα1 and Impα2, indicating that there might be other positions in the P5 involved in its nucleus targeting. Furthermore, BiFC assays were performed for P5 and nucleolus fibrillarin protein Fib2. The nucleus marker H2B-mCherry was not included in the test to avoid its effect on the location evaluation. It was found that P5 and Fib2 interacted with signal in the nucleolus and in nucleus as small bodies, but not in the nucleoplasm (Figure 6c), indicating that the P5 located in the nucleolus and NBs by interaction with Fib2.

2.7 | Dissection of the P5 determinants for its subcellular localizations and systemic RNA silencing suppression activity

To assess whether specific regions of P5 are necessary for its subcellular localizations and self-interaction, four YFP-tagged mutants $P5_{1-89}$, $P5_{20-89}$, $P5_{20-282}$ and $P5_{90-282}$ were constructed

according to the secondary structure and the SP position of P5 protein (Figure S6b,c) and transiently co-expressed with nuclear, PD and ER marker proteins H2B-mCherry, CMV 3a-mCherry and mCherry-HDEL in *N. benthamiana* by *A. tumefaciens*-mediated transformation. The fluorescence signals in the infiltrated leaf patches were examined at 2 dpi (Figure 7a). The mutants $P5_{1-89}$ and $P5_{20-89}$ had subcellular locations similar to that of full-length P5 with YFP signal in the nucleoplasm without forming NBs, at PD and ER, where it induced many vesicles. The signal of the mutant $P5_{20-282}$ located in the nucleus with NBs and PD, but lost ER location, and formed many granular structures in the ER networks. The $P5_{90-282}$ location was much different from that of full-length P5 by losing PD location, forming many multiple vesicle structures. The $P5_{90-282}$ changed the ER structure, which appeared as granular structures in the $P5_{90-282}$ vesicles (Figure 7a). Further BiFC assays revealed the self-interaction of $P5_{1-89}$ with interaction fluorescence signal at the same locations as the full-length P5, but other mutants failed to self-interact (Figure 7b, Figure S7). The LCI tests also confirmed the $P5_{1-89}$ self-interaction (Figure 7c).

To determine whether specific regions or motifs of P5 are necessary for suppressing RNA silencing, the systemic suppression ability of the four mutants was determined (Figure 8a). Results showed that $P5_{1-89}$ successfully suppressed systemic silencing in *N. benthamiana* 16c plants. At 35 dpi, nine of 10 $P5_{1-89}$/35S:GFP-infiltrated plants showed no systemic silencing with the GFP fluorescence signal visible in apical leaves similar to the full-length P5. The SP deletion
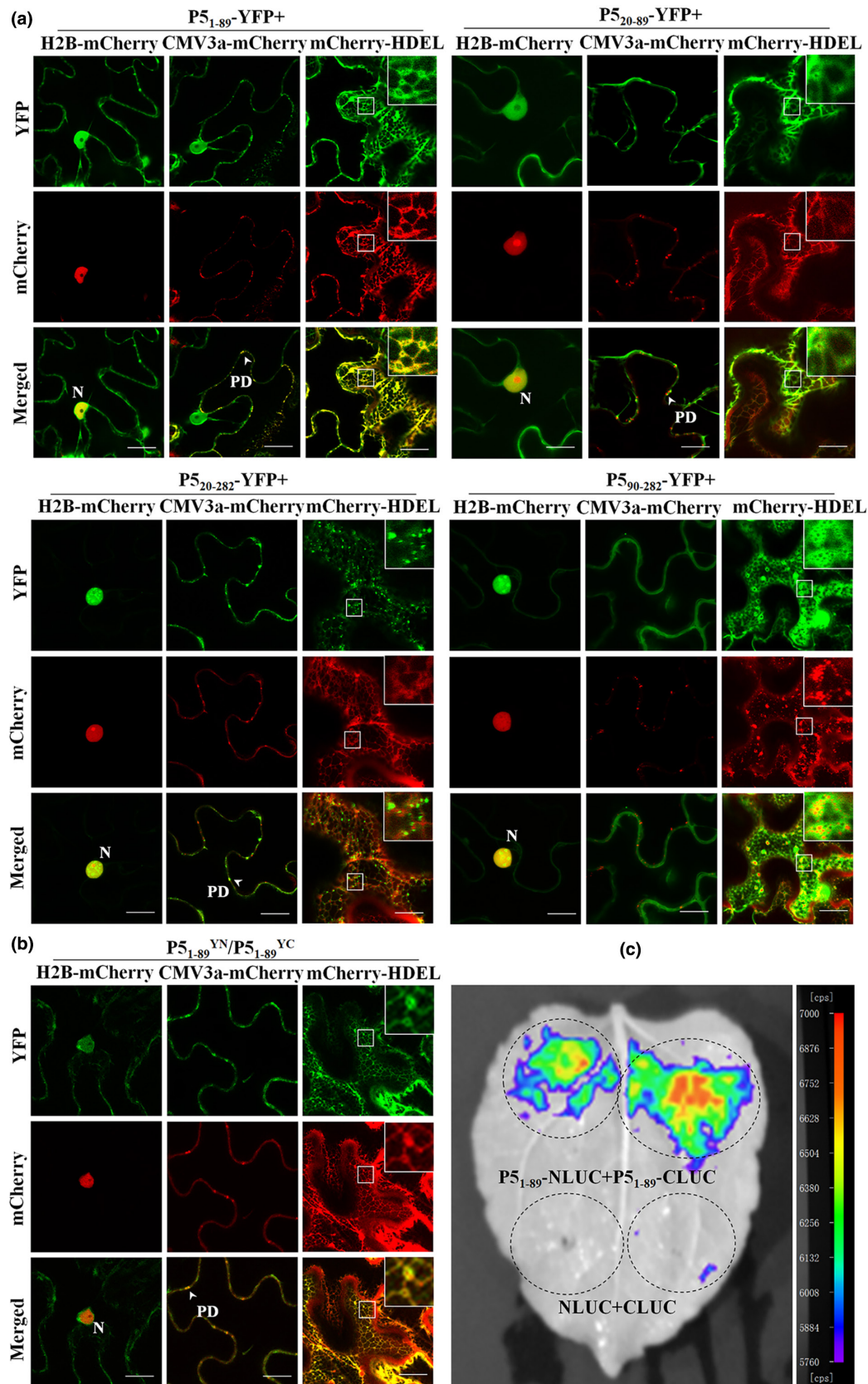
FIGURE 7 Subcellular colocalization features of truncated PCLSaV P5 mutants (a) and the self-interaction of mutant $P5_{1-89}$ detected by bimolecular fluorescence complementation and luciferase complementation assays in *Nicotiana benthamiana* epidermal cells (b, c). In (a, b), CMV3a-mCherry, H2B-mCherry and mCherry-HDEL were used as plasmodesmata, nuclear and endoplasmic reticulum markers. The endoplasmic reticulum structures with colocalization signals were highlighted in the boxes. N, nucleus; PD, plasmodesmata. Images were acquired at 48h after agroinfiltration under a confocal microscope using a 63×/1.20 water objective. Scale bars=20μm.
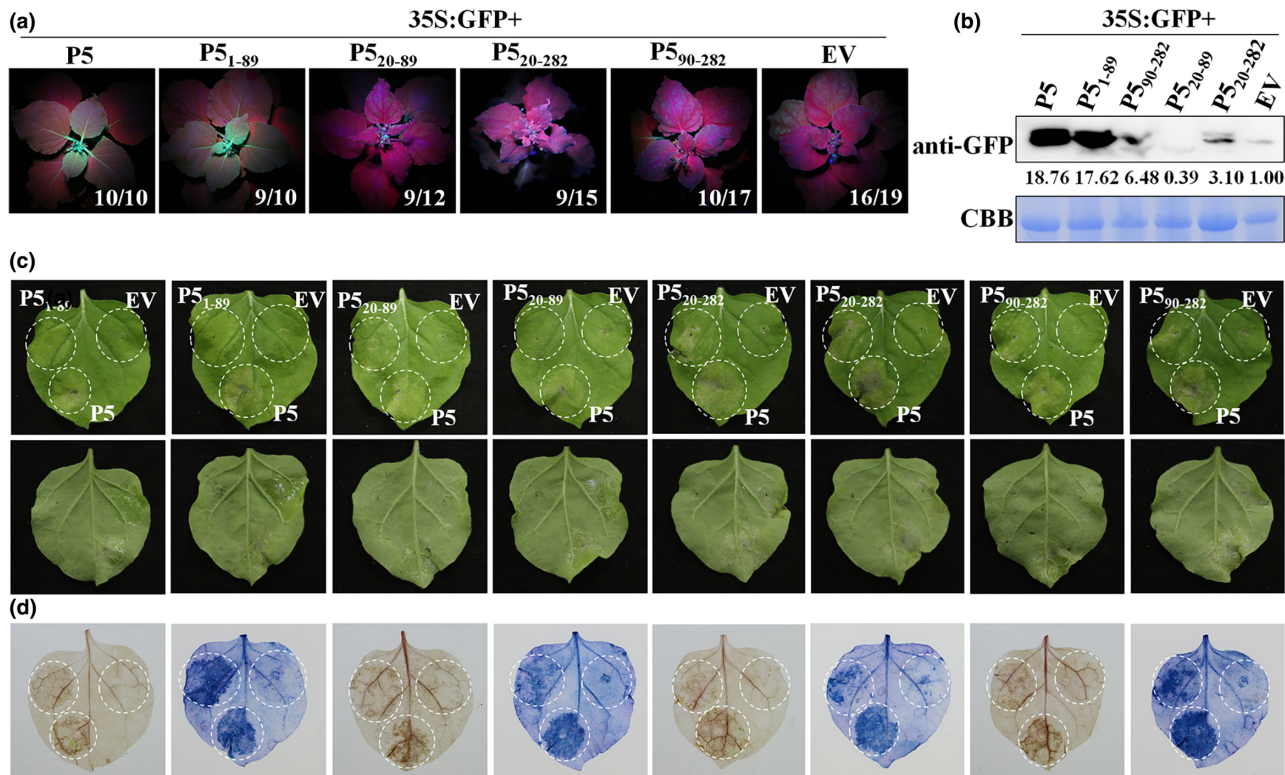
FIGURE 8 RNA silencing suppression and reactive oxygen species induction activities of truncated PCLSaV P5 mutants in *Nicotiana benthamiana* line 16c. (a, b) The signals and accumulation levels of GFP in systemic leaves of *N. benthamiana* line 16c infiltrated with P5 and P5 mutants. The numbers in (a) indicated the ratios of plants showing the corresponding phenotypes and total tested plants. In (b), the large subunit of RuBisCO stained with Coomassie brilliant blue (CBB) is used as a protein loading control. (c) Phenotypes of *N. benthamiana* leaf patches infiltrated with P5 and its mutants (upper panel, front; lower panel, back). (d) The 3.3′-diaminobenzidine (DAB) (left) and trypan blue (right) staining of leaves shown in (c).

($P5_{20-89}$ and $P5_{20-282}$) greatly abolished the suppression activity of $P5_{1-89}$ and P5, with 75% (9/12) and 60% (9/15) plants showing a systemic GFP silencing phenotype. The mutant protein $P5_{90-282}$ largely lost its suppression activity with 59% (10/17) infiltrated plants showing the systemic silencing phenotype. Consistent with the phenotypes, the GFP accumulation level in systemic leaves of plants infiltrated with $P5_{1-89}$ was comparable to that of P5-infiltrated plants and was much higher than that of plants infiltrated with EV and other three mutants (Figure 8b).

Furthermore, the abilities of these mutants inducing chlorotic necrosis and ROS accumulation were assessed in wild-type *N. benthamiana* plants (Figure 8c,d). All leaf patches infiltrated with these mutants produced the same chlorotic necrosis as that induced by the full-length P5 (Figure 8c). DAB and NBT staining revealed that dark brown and deep blue colours developed in leaf patches infiltrated with these mutants, although the colour intensities in patches infiltrated with mutants $P5_{20-89}$, $P5_{20-282}$ and $P5_{90-282}$ were slightly weaker than that in $P5_{1-89}$ and P5-infiltrated patches (Figure 8d).

Collectively, these data suggested that the 1–89 aa at the N terminus of P5 is responsible for the PD location; the formation of ER-derived vesicles, self-interaction and RNA silencing suppressor (RSS)

activity; and the SP is indispensable for the self-interaction and RSS activity.

3 | DISCUSSION

Emaraviruses harbour RNAs encoding divergent and unique proteins. The PCLSaV RNA5 is highly expressed in virus-infected pear leaves as assayed by RNA-Seq (Liu et al., 2020), indicating that the protein P5 encoded by the viral genomic RNA5 might be involved in specific biological functions. Here, we demonstrated the roles of PCLSaV P5 in pathogenicity and movement. Most RSSs can block either local silencing or systemic silencing or both (Hamilton et al., 2002). This study provided evidence that P5 is an RSS, with mild activity for suppressing local RNA silencing, but strong activity for suppressing systemic RNA silencing. As a systemic RNA silencing suppressor, the protein P5 can efficiently block systemic spread of silencing inducing signals, as shown by transient agro-expression and expression via a heterologous PVX vector, and the activity is comparable with the well-known RSS P19 of TBSV (Qiu et al., 2002). dsRNA is a strong inducer of RNA silencing (Fire et al., 1998). Our results also showed that P5 partially suppresses

local silencing induced by GFP dsRNA, but not by ssRNA. This is the second report of an emaravirus protein as a silencing suppressor. The P7 and P8 of the emaravirus HPWMoV were previously identified as RSSs efficiently suppressing the transitive pathway of silencing (Gupta et al., 2018). The known virus RSSs are highly divergent in sequences and function in different steps of RNA silencing (Li & Wang, 2019; Pumplin & Voinnet, 2013). The PCLSaV P5 is distantly related to P7 of HPWMoV (Liu et al., 2020), but does not have a glycine-tryptophan (GW) motif, which is considered to be necessary for the RSS activity of HPWMoV P7 (Gupta et al., 2018) and many other RSSs (Genovés et al., 2010; Gupta et al., 2019; Weber & Bujarski, 2015). The mechanism of the PCLSaV P5 affecting RNA silencing pathway remains to be elucidated.

The infections of many plant viruses cause chlorosis, chlorotic spots and necrosis, which are manifestations of the immune responses in infected cells. Rapid generation of ROS, such as H_2O_2 or O^-_2, is one of the earliest cellular responses against pathogen infections (Bolwell & Wojtaszek, 1997). The RSSs encoded by many plant viruses are effective effectors, stimulating the immune response of plants (Culver & Padmanabhan, 2007; Nakahara & Masuta, 2014; Pallas & García, 2011). There is some evidence to suggest that ROS bursts are correlated with successful plant virus infection and disease development (Díaz-Vivancos et al., 2008). Viruses can promote their own infection or replication by regulating ROS via various pathways (Hyodo et al., 2017; Jiao et al., 2021; Yang et al., 2020, 2022). The well-known RSS P19 of TBSV can trigger the host hypersensitive reaction and a ROS burst (Scholthof, 2006). This study showed that the P5 expression induced ROS production and chlorosis or necrosis of *N. benthamiana* leaf patches, consistent with PCLSaV infection in pear that commonly induced semitransparent chlorotic spots and necrotic flecks (Liu et al., 2020). The RSS activity and ROS induction of P5 might play an important role in facilitating virus infection. In accordance with the activity of P5 in suppressing RNA silencing and ROS induction, P5 could improve the accumulation and enhance the pathogenicity of a heterologous PVX, when expressed through the heterologous virus vector, as described for some other RSSs (Samuel et al., 2016; Tatineni et al., 2012). Similar roles in enhancing heterologous virus infection have been previously reported for RLBV P6 and P7 (Lu et al., 2015) and HPWMoV P7 and P8 (Gupta et al., 2018). However, the pathways these emaravirus proteins interfere with remain to be further elucidated. With the establishment of a rose rosette virus (RRV) infectious clone (Verchot et al., 2020), reverse genetics studies will improve our understanding of the biological functions of emaravirus unique proteins.

The biochemical and molecular pathways underlying the pathogenicity role of emaravirus proteins are unknown. Discerning the subcellular localization of a protein is crucial for understanding its biological role. Interestingly, P5 localized in the nuclear, ER and PD, indicating the protein might play multiple roles in the virus infection cycle. Furthermore, P5 had the ability to rescue the cell-to-cell movement of a movement-deficient virus PVXΔP25, suggesting that

P5 might be essential for the virus movement. The PCLSaV P4 was assumed to be the viral MP based on its significant sequence similarity with the P4 proteins of RLBV and some other emaraviruses (Liu et al., 2020; Yu et al., 2013). The distribution of MPs at PD has been described for some emaraviruses, but its biological role was not evaluated (McGavin et al., 2012). In the present study, we found that transiently expressed PCLSaV P4 localized to PD and also facilitated cell-to-cell trafficking of a movemen-defective PVXΔP25, confirming that the P4 functions in the virus movement. Moreover, P5 interacted with P4 at PD. As some other viruses, with two or more proteins involved in virus movement (Guo et al., 2020), P5 might cooperate with P4 in the PCLSaV movement. The coordinated replication and intercellular movement of some plant viruses are associated with the ER and mediated by membrane-associated motile vesicular structures (Li et al., 2024; Linnik et al., 2013; Tilsner et al., 2012, 2013; Tilsner & Oparka, 2012). Many plant RNA viruses and their movement proteins are associated with the ER network of their hosts, and the ER is involved in virus movement and viral replication complex formation (Bamunusinghe et al., 2011; Feng et al., 2019). In the present study, we found that P5 was associated with endoplasmic membrane structures, in which many vesicles were induced, suggesting that P5 might use the plant cytoskeleton to mediate the movement of viral replication complexes (VCRs) from their replication sites to PD (Naghavi & Walsh, 2017).

This study also demonstrated that the PCLSaV P5 increased PVX CP expression, further supporting that P5 is a silencing suppressor like TBSV P19, which has been used to suppress host antiviral defences and to increase GFP or viral clone expression (Feng et al., 2019; Ganesan et al., 2013; Qian et al., 2017). As the full-length P5, the self-interaction and the nucleus, ER and PD locations of the deletion mutant $P5_{1-89}$ were documented in BiFC assays (Figure 7b). Importantly, the $P5_{1-89}$ alone could efficiently lead to suppress systemic RNA silencing, which was comparable to the full-length P5 (Figure 8a), indicating that the stable dimers might be necessary for its functions (Chou et al., 2013). From a structural perspective, P5 contains a putative SP consisting of 19 aa at the N terminus, which was confirmed by its secretion function. Truncation of the SP from the full-length P5 and the $P5_{1-89}$ abolished their self-interaction and greatly decreased their VSR activity, suggesting that the SP was indispensable for the silencing function. Although an NLS was predicted at positions 203–233 aa, the deletions of C terminus ($P5_{1-89}$) and NLS sequences of P5 did not abolish their nuclear localization and nuclear transport by the importin α pathway, suggesting that there might be functional nuclear localization sites also at its N terminus. In addition, the RSS activity and subcellular location feature of P5 were not strictly related as revealed by transient agro-expression of truncated P5 mutant $P5_{20-89}$, which showed subcellular locations similar to P5 and $P5_{1-89}$ in *N. benthamiana*, but did not show detectable RSS activity.

In summary, we explored the biological functions of PCLSaV P5. This study provided evidence for dual roles of a unique protein of an emaravirus in countering plant antiviral defence by suppressing plant RNAi and in facilitating virus movement.

4 | EXPERIMENTAL PROCEDURES

4.1 | Plant growth condition and virus inoculation

Nicotiana benthamiana (wild-type and line 16c) plants were grown in a chamber in 60% relative humidity with a 16-h daylight period at 25°C and an 8-h dark period at 20°C. The leaf sample of a *P. pyrifolia* 'Cuiguan' plant, from which the genome of PCLSaV isolate CG1 was identified (Liu et al., 2020), was used for the amplification of the virus protein coding sequences.

For PVX inoculation, the recombinant PVX infectious clone was transformed into *A. tumefaciens* GV3101 by a heat shock method. After incubating in Luria Bertani (LB) broth at 28°C, the cultures (OD$_{600nm}$ = 1) were centrifuged and resuspended with an infiltration buffer (10 mM MES, pH 5.7, 10 mM MgCl$_2$, 100 μM acetosyringone) to a final OD$_{600nm}$ of 0.5. To enhance PVX mutant PVXΔ25-GFP infection, *Agrobacterium* culture (OD$_{600nm}$ = 0.8) expressing TBSV P19, a strong silencing suppressor, was mixed with the PVXΔ25-GFP culture. After incubating at 25°C for 2 h, the suspensions or mixtures were infiltrated into leaves of 4-week-old *N. benthamiana* plants.

4.2 | Gene cloning and sequences analysis

The coding sequences (ORFs 2–5) of PCLSaV proteins were amplified individually from CG1 sample by reverse transcription (RT)-PCR using primers designed from the genome sequences of PCLSaV isolate CG1 (GenBank accession nos. MK602177 to MK602181 for RNA1 to RNA5). Within ORF2, two fragments encoding GN and GC were amplified using primers designed based on the predicted restriction digestion sites (Liu et al., 2020). The RT-PCR conditions were the same as previously reported (Liu et al., 2020). The PCR products were purified and ligated into the pMD18-T vector (TaKaRa). Clones were identified by PCR and at least three recombinant clones of each product were sequenced at Sangon Biotech (Shanghai) Co., Ltd., Shanghai, China. One clone of each amplicon with a consensus sequence was selected for further study. The primers used in PCR are listed in Table S2.

4.3 | BiFC, LCI and subcellular localization assays

The construction of vectors used for BiFC and subcellular localization assays was performed using the Gateway Technology (Invitrogen), as previously described (Yang et al., 2021). In BiFC assays, sequence-validated entry clones (without the stop codon) were individually recombined into the pEarlygate201-YN or pEarlygate202-YC vectors using the Gateway LR Clonase II Enzyme mix. The vector pEarlyGate101-eYFP was used for subcellular localization. The cloned genes were individually fused to the N terminus of eYFP (Yang et al., 2021).

In BiFC and subcellular localization assays, the plasmids expressing mCherry-HDEL (Feng et al., 2019), H2B-mCherry (Martin et al., 2009) and CMV3a-mCherry (Ur Rehman et al., 2019) were used as ER, nucleus and PD markers, respectively. All constructs were transformed into *A. tumefaciens* GV3101 cells (Weidi Bio) using a heat shock method. The transformed *A. tumefaciens* cells were resuspended in infiltration buffer (10 mM MgCl$_2$, 10 mM MES, 150 μM acetosyringone), incubated at 28°C for 2–5 h (OD$_{600nm}$ = 0.7) and then infiltrated into *N. benthamiana* leaves with needleless syringes, as previously described (Yang et al., 2021). In BiFC assays, P19 was used as a positive control and the empty vector (EV) was used as a negative control. The infiltrated leaf sections were visualized at 48 hpi under a laser scanning confocal microscopy (LSCM; TCS-SP8, Leica Microsystems) with an HC PL APO CS2 63×/1.20 water objective. CFP, YFP and mCherry fluorescence signals were excited at wavelengths 458 nm, 514 nm and 561 nm and captured at wavelengths 470–510 nm, 524–544 nm and 580–600 nm, respectively.

For LCI assays, each coding sequence was inserted into pJW771-nLUC and pJW772-cLUC vectors by using a ClonExpress II One Step Cloning Kit (Vazyme). *Agrobacterium* cultures harbouring paired plasmids were co-infiltrated into *N. benthamiana* leaves. At 48–60 hpi, the luciferase substrate D-luciferin solution (0.2 mM) (GlpBio) was sprayed onto the surface of infiltrated leaves. About 5–10 min later, the luciferase activity was detected using a low-light cooled CCD imaging apparatus (NightSHADE L985; Berthold).

4.4 | Identification of viral RNA silencing suppressors

To determine RNA silencing suppression activity, the PCLSaV ORFs were constructed into the vector FLAG-tagged pCNF3 (Ur Rehman et al., 2019). The vectors were constructed by using the ClonExpress II One Step Cloning Kit (Vazyme). Each recombinant vector was transformed into *A. tumefaciens* GV3101 cells. An *Agrobacterium* culture containing a plasmid pMS4 (with a 35S:GFP) was used as an inducer of RNA silencing. The well-known suppressor P19 of TBSV was used as a positive control. The empty pCNF3 vector was used as a negative control. *Agrobacterium* cultures transformed with each of the constructs were individually co-infiltrated with a culture carrying 35S:GFP at a ratio of 1:1 (vol/vol) into the leaves of GFP-expressing *N. benthamiana* 16c for local and systemic silencing tests. Each assay was repeated at least three times. Local GFP expression signals were monitored at 2–6 dpi, and systemic GFP expression signals were monitored at 14–40 dpi under a hand-held UV lamp (LUYOR-3104). Images were captured using a camera (EOS 450D; Canon). The green fluorescence signals observed in the young leaves of infiltrated plants were quantified as systemic RNA silencing suppression.

4.5 | Immunoblot analysis

The protein extraction and immunoblot assays were performed as previously described (Yang et al., 2021). Monoclonal antibody

against GFP (Sangon Biotech [Shanghai] Co., Ltd.) was used at a dilution of 1:5000. Anti-PVX CP antibody was kindly provided by Professor Tao Zhou (China Agricultural University) and used at a dilution of 1:5000. The large subunit of RuBisCO stained by Coomassie brilliant blue (CBB) was used as protein loading controls in western blot assays.

4.6 | RNA extraction and RT-qPCR analysis

Total RNA was extracted from *N. benthamiana* leaf samples using TRIzol reagent (Invitrogen) and treated with DNase I (TaKaRa). First-strand cDNA was synthesized by using All-In-One RT MasterMix (with AccuRT Genomic DNA Removal Kit) (Abm). All qPCR assays were performed using the iTaq Universal SYBR Green Supermix (Bio-Rad) in a CFX96 real-time system (Bio-Rad), as previously described (Yang et al., 2021). The *N. benthamiana* NbGAPDH gene (GenBank accession no. JQ256517.1) was used as internal control. The relative expression levels were calculated by using the cycle threshold (C_t) $2^{-\Delta\Delta Ct}$ method (Livak & Schmittgen, 2001). All experiments were replicated at least three times. The primers used for the RT-qPCR assays of *NbPR1*, *NbPR4*, *NbGAPDH* and *GFP* gene expression levels were listed in Table S3.

4.7 | Hydrogen peroxide content measurements, trypan blue and DAB staining

The H_2O_2 content was measured using the micromethod kit following the manufacturer's instructions (Nanjing Molfarming Biotech Co.). The infiltrated dishes with a diameter of 0.5 cm were placed in the wells of 96-well plates with 0.1-mL double-distilled water and incubated for 10 h at room temperature. After removing the double-distilled water, 0.1-mL reaction mixture (containing 50 μM luminol [L-012] and 10 μg/mL peroxidase) was added to each well. Then, the absorbance value of each solution in the plate wells was tested at A_{488nm} as the excitation wavelength and A_{525nm} as the emission wavelength. The reaction was measured at 90-s intervals, and the readings were repeated 30 times for a total of 45 min in one cycle. The values of ROS produced by the treated leaf discs were calculated as relative light unit (RLU) using Prism software (v. 8.0.2). Three biological replicates were designed in each tested group.

For trypan blue staining, infiltrated leaves of *N. benthamiana* were immersed in trypan blue staining solution (30 mL ethanol, 10 mL phenol, 10 mL sterile water, 10 mL glycerol, 10 mL lactic acid, 20 mg trypan blue) and boiled in a water bath for 3 min, then destained in 100% ethanol at room temperature for 24 h.

For DAB staining, 30 mg DAB mixed with 30 mL of sterile water (with hydrochloric acid to accelerate dissolution) to a final concentration of 1 mg/mL (pH 3.8) (protected from light). Infiltrated leaves of *N. benthamiana* were immersed DAB solution for 16–20 h, then washed with water two or three times and destained in 100% ethanol at room temperature for about 24 h.

4.8 | Quantification and statistical analysis

Statistical significance was examined by one-sided Student's t test or one-way analysis of variance with Dunnett's multiple comparison test. The values for quantitative analysis were shown as mean $\pm SD$ from at least three independent assays. Asterisks indicate significant difference (*$p < 0.05$, **$p < 0.01$, ***$p < 0.001$). The blotted bands were quantified using ImageJ and normalized against that of the loading control from the same sample.

CONFLICT OF INTEREST STATEMENT

The authors have no conflicts of interest.

DATA AVAILABILITY STATEMENT

The data that support the findings of this study are available from the corresponding author upon reasonable request.

ORCID

Ni Hong https://orcid.org/0000-0002-1285-4455

REFERENCES

Bamunusinghe, D., Seo, J.K. & Rao, A.L.N. (2011) Subcellular localization and rearrangement of endoplasmic reticulum by brome mosaic virus capsid protein. *Journal of Virology*, 85, 2953–2963.

Bolwell, G.P. & Wojtaszek, P. (1997) Mechanisms for the generation of reactive oxygen species in plant defence – a broad perspective. *Physiological and Molecular Plant Pathology*, 51, 347–366.

Chou, Y.L., Hung, Y.J., Tseng, Y.H., Hsu, H.T., Yang, J.Y., Wung, C.H. et al. (2013) The stable association of virion with the triple-gene-block protein 3-based complex of bamboo mosaic virus. *PLoS Pathogens*, 9, e1003405.

Culver, J.N. & Padmanabhan, M.S. (2007) Virus-induced disease: altering host physiology one interaction at a time. *Annual Review of Phytopathology*, 45, 221–243.

Di Bello, P.L., Laney, A.G., Druciarek, T., Ho, T., Gergerich, R.C., Keller, K.E. et al. (2016) A novel emaravirus is associated with redbud yellow ringspot disease. *Virus Research*, 222, 41–47.

Díaz-Vivancos, P., Clemente-Moreno, M.J., Rubio, M., Olmos, E., García, J.A., Martínez-Gómez, P. et al. (2008) Alteration in the chloroplastic metabolism leads to ROS accumulation in pea plants in response to plum pox virus. *Journal of Experimental Botany*, 59, 2147–2160.

Digiaro, M., Elbeaino, T., Kubota, K., Ochoa-Coron, F.M. & von Bargen, S. (2024) ICTV virus taxonomy profile: *Fimoviridae* 2024. *Journal of General Virology*, 105, 1943.

Elbeaino, T., Digiaro, M., Mielke-Ehret, N., Muehlbach, H.P. & Martelli, G.P. (2018) ICTV virus taxonomy profile: *Fimoviridae*. *Journal of General Virology*, 99, 1478–1479.

Feng, M.F., Cheng, R.X., Chen, M.L., Guo, R., Li, L.Y., Feng, Z.K. et al. (2019) Rescue of tomato spotted wilt tospovirus entirely from cDNA clones, establishment of the first reverse genetics system

for a segmented (−) RNA plant virus. *Proceedings of the National Academy of Sciences of the United States of America*, 117, 1181–1190.

Fire, A., Xu, S., Montgomery, M.K., Kostas, S.A., Driver, S.E. & Mello, C.C. (1998) Potent and specific genetic interference by double-stranded RNA in *Caenorhabditis elegans*. *Nature*, 391, 806–811.

Ganesan, U., Bragg, J.N., Deng, M., Marr, S., Lee, M.Y., Qian, S.S. et al. (2013) Construction of a Sonchus yellow net virus minireplicon: a step toward reverse genetic analysis of plant negative-strand RNA viruses. *Journal of Virology*, 87, 10598–10611.

Genovés, A., Navarro, J.A. & Pallás, V. (2010) The intra-and intercellular movement of melon necrotic spot virus (MNSV) depends on an active secretory pathway. *Molecular Plant–Microbe Interactions*, 23, 263–272.

Goldfarb, D.S., Corbett, A.H., Mason, D.A., Harreman, M.T. & Adam, S.A. (2004) Importin α: a multipurpose nuclear-transport receptor. *Trends in Cell Biology*, 14, 505–514.

Guo, J.S., Wang, Y.X., Wang, G.P., Hong, J., Yang, Z.K., Bai, J.Y. et al. (2020) Molecular characteristics of jujube yellow mottle-associated virus infecting jujube (*Ziziphus jujuba* Mill.) grown at Aksu in Xinjiang of China. *Viruses*, 13, 25.

Gupta, A.K., Hein, G.L., Graybosch, R.A. & Tatineni, S. (2018) Octopartite negative-sense RNA genome of High Plains wheat mosaic virus encodes two suppressors of RNA silencing. *Virology*, 518, 152–162.

Gupta, A.K., Hein, G.L. & Tatineni, S. (2019) P7 and P8 proteins of High Plains wheat mosaic virus, a negative-strand RNA virus, employ distinct mechanisms of RNA silencing suppression. *Virology*, 535, 20–31.

Hamilton, A., Voinnet, O., Chappell, L. & Baulcombe, D. (2002) Two classes of short interfering RNA in RNA silencing. *The EMBO Journal*, 21, 4671–4679.

Hassan, M., Di Bello, P.L., Keller, K.E., Martinc, R.R., Sabanadzovic, S. & Tzanetakis, I.E. (2017) A new, widespread emaravirus discovered in blackberry. *Virus Research*, 235, 1–5.

Hyodo, K., Hashimoto, K., Kuchitsu, K., Suzuki, N. & Okuno, T. (2017) Harnessing host ROS-generating machinery for the robust genome replication of a plant RNA virus. *Proceedings of the National Academy of Sciences of the United States of America*, 114, E1282–E1290.

Ishikawa, K., Maejima, K., Komatsu, K., Netsu, O., Keima, T., Shiraishi, T. et al. (2013) Fig mosaic emaravirus P4 protein is involved in cell-to-cell movement. *Journal of General Virology*, 94, 682–686.

Jiao, Z.Y., Tian, Y.Y., Cao, Y.Y., Wang, J., Zhan, B.H., Zhao, Z.X. et al. (2021) A novel pathogenicity determinant hijacks maize catalase 1 to enhance viral multiplication and infection. *New Phytologist*, 230, 1126–1141.

Kubota, K., Chiaki, Y., Yanagisawa, H., Takeyama, S., Suzuki, R., Kohyama, M. et al. (2021) First report of pear chlorotic leaf spot-associated virus on Japanese and European pears in Japan and its detection from an eriophyid mite. *Plant Disease*, 105, 1234.

Lange, A., Mills, R.E., Lange, C.J., Stewart, M., Devine, S.E. & Corbett, A.H. (2007) Classical nuclear localization signals: definition, function, and interaction with importin α. *Journal of Biological Chemistry*, 282, 5101–5105.

Li, F.F. & Wang, A. (2019) RNA-targeted antiviral immunity: more than just RNA silencing. *Trends in Microbiology*, 27, 792–805.

Li, L., Wang, G.P., Zhang, Y., Wang, W.J., Zhu, Y.T., Lyu, Y.Z. et al. (2024) The functions of triple gene block proteins and coat protein of apple stem pitting virus in viral cell-to-cell movement. *Molecular Plant Pathology*, 25, e13392.

Linnik, O., Liesche, J., Tilsner, J. & Oparka, K.J. (2013) Unraveling the structure of viral replication complexes at super-resolution. *Frontiers in Plant Science*, 4, 6.

Liu, H.Z., Wang, G.P., Yang, Z.K., Wang, Y.X., Zhang, Z., Li, L.H. et al. (2020) Identification and characterization of a pear chlorotic leaf spot-associated virus, a novel emaravirus associated with a severe disease of pear trees in China. *Plant Disease*, 104, 2786–2798.

Livak, K.J. & Schmittgen, T.D. (2001) Analysis of relative gene expression data using real-time quantitative PCR and the $2^{-\Delta\Delta CT}$ method. *Methods*, 25, 402–408.

Lu, Y.W., McGavin, W., Cock, J.A., Schnettler, E., Yan, F., Chen, J.P. et al. (2015) Newly identified RNAs of raspberry leaf blotch virus encoding a related group of proteins. *Journal of General Virology*, 96, 3432–3439.

Martin, K.M., Kopperud, K., Chakrabarty, R., Banerjee, R., Brooks, R. & Goodin, M.M. (2009) Transient expression in *Nicotiana benthamiana* fluorescent marker lines provides enhanced definition of protein localization, movement and interactions in planta. *The Plant Journal*, 59, 150–162.

McGavin, W.J., Mitchell, C., Cock, P.J., Wright, K.M. & MacFarlane, S.A. (2012) Raspberry leaf blotch virus, a putative new member of the genus *Emaravirus*, encodes a novel genomic RNA. *Journal of General Virology*, 93, 430–437.

Mielke-Ehret, N. & Mühlbach, H.P. (2012) *Emaravirus*: a novel genus of multipartite, negative strand RNA plant viruses. *Viruses*, 4, 1515–1536.

Mühlbach, H.P. & Mielke-Ehret, N. (2012) Emaravirus. In: King, A.M.Q. et al. (Eds.) *Virus taxonomy. Classification and nomenclature of viruses. Ninth report of the International Committee on Taxonomy of Viruses*. London: Elsevier Academic Press, pp. 767–770.

Naghavi, M.H. & Walsh, D. (2017) Microtubule regulation and function during virus infection. *Journal of Virology*, 91, 1110–1128.

Nakahara, K.S. & Masuta, C. (2014) Interaction between viral RNA silencing suppressors and host factors in plant immunity. *Current Opinion in Plant Biology*, 20, 88–95.

Pallas, V. & García, J.A. (2011) How do plant viruses induce disease? Interactions and interference with host components. *Journal of General Virology*, 92, 2691–2705.

Pumplin, N. & Voinnet, O. (2013) RNA silencing suppression by plant pathogens: defense, counter-defense and counter-counter-defense. *Nature Reviews Microbiology*, 11, 745–760.

Qian, S.S., Chen, X.L., Sun, K., Zhang, Y. & Li, Z.H. (2017) Capped antigenomic RNA transcript facilitates rescue of a plant rhabdovirus. *Journal of Virology*, 14, 1–12.

Qiu, W.P., Park, J.W. & Scholthof, H.B. (2002) Tombusvirus P19-mediated suppression of virus-induced gene silencing is controlled by genetic and dosage features that influence pathogenicity. *Molecular Plant–Microbe Interactions*, 15, 269–280.

Rehanek, M., Karlin, D.G., Bandte, M., Al Kubrusli, R., Nourinejhad Zarghani, S., Candresse, T. et al. (2022) The complex world of emaraviruses – challenges, insights, and prospects. *Forests*, 13, 1868.

Samuel, G.H., Wiley, M.R., Badawi, A., Adelman, Z.N. & Myles, K.M. (2016) Yellow fever virus capsid protein is a potent suppressor of RNA silencing that binds double-stranded RNA. *Proceedings of the National Academy of Sciences of the United States of America*, 113, 13863–13868.

Scholthof, H.B. (2006) The tombusvirus-encoded P19: from irrelevance to elegance. *Nature Reviews Microbiology*, 4, 405–411.

Tatineni, S., Mcmechan, A.J., Wosula, E.N., Wegulo, S.N., Graybosch, R.A., French, R. et al. (2014) An eriophyid mite-transmitted plant virus contains eight genomic RNA segments with unusual heterogeneity in the nucleocapsid protein. *Journal of Virology*, 88, 11834–11845.

Tatineni, S., Qu, F., Li, R., Morris, T.J. & French, R. (2012) Triticum mosaic poacevirus enlists P1 rather than HC-pro to suppress RNA silencing-mediated host defense. *Virology*, 433, 104–115.

Thaminy, S., Auerbach, D., Arnoldo, A. & Stagljar, I. (2003) Identification of novel ErbB3-interacting factors using the split-ubiquitin membrane yeast two-hybrid system. *Genome Research*, 13, 1744–1753.

Tilsner, J., Linnik, O., Louveaux, M., Roberts, I.M., Chapman, S.N. & Oparka, K.J. (2013) Replication and trafficking of a plant virus are coupled at the entrances of plasmodesmata. *Journal of Cell Biology*, 201, 981–995.

Tilsner, J., Linnik, O., Wright, K.M., Bell, K., Roberts, A.G., Lacomme, C. et al. (2012) The TGB1 movement protein of potato virus X reorganizes actin and endomembranes into the X-body, a viral replication factory. *Plant Physiology*, 158, 1359–1370.

Tilsner, J. & Oparka, K.J. (2012) Missing links? The connection between replication and movement of plant RNA viruses. *Current Opinion in Virology*, 2, 705–711.

Ur Rehman, A., Li, Z.R., Yang, Z.K., Waqas, M.M., Wang, G.P., Xu, W.X. et al. (2019) The coat protein of citrus yellow vein clearing virus interacts with viral movement proteins and serves as an RNA silencing suppressor. *Viruses*, 11, 329.

Verchot, J., Herath, V., Urrutia, C.D., Gayral, M., Lyle, K., Shires, M.K. et al. (2020) Development of a reverse genetic system for studying rose rosette virus in whole plants. *Molecular Plant–Microbe Interactions*, 33, 1209–1221.

Weber, P.H. & Bujarski, J.J. (2015) Multiple functions of capsid proteins in (+) stranded RNA viruses during plant–virus interactions. *Virus Research*, 196, 140–149.

Yang, D.Y., Peng, Q.D., Cheng, Y.C. & Hui, D. (2022) Glucose-6-phosphate dehydrogenase promotes the infection of Chilli veinal mottle virus through affecting ROS signaling in *Nicotiana benthamiana*. *Planta*, 256, 96.

Yang, T., Qiu, L., Huang, W.Y., Xu, Q.Y., Zou, J.L., Peng, Q.D. et al. (2020) Chilli veinal mottle virus HCPro interacts with catalase to facilitate virus infection in *Nicotiana tabacum*. *Journal of Experimental Botany*, 71, 5656–5668.

Yang, Z.K., Zhang, Y.L., Wang, G.P., Wen, S.H., Wang, Y.X., Li, L. et al. (2021) The p23 of citrus tristeza virus interacts with host FKBP-type peptidyl-prolylcis-trans isomerase 17-2 and is involved in the intracellular movement of the viral coat protein. *Cells*, 10, 934.

Yu, C., Karlin, D.G., Lu, Y., Wright, K., Chen, J. & MacFarlane, S. (2013) Experimental and bioinformatic evidence that raspberry leaf blotch emaravirus P4 is a movement protein of the 30K superfamily. *Journal of General Virology*, 94, 2117–2128.

Zheng, Y.Z., Wang, G.P., Zhou, J.F., Zhu, C.X., Wang, L.P., Xu, W.X. et al. (2015) Detection and molecular variation of kiwifruit virus A and B by RT-PCR. *Chinese Journal of Horticulture*, 42, 665–671.

Zhu, Y.T., Hong, N., Li, L., Gao, Y.J., Wang, L.P., Xu, W.X. et al. (2022) Development of a sensitive real-time quantitative RT-PCR assay for the detection of pear chlorotic leaf spot-associated virus. *Journal of Virology Methods*, 309, 114608.

SUPPORTING INFORMATION

Additional supporting information can be found online in the Supporting Information section at the end of this article.